ChemComm

Interactions of CO and/or H2O with mesoporous oxide-supported metal catalysts: the role of MSI effects

Journal:	*ChemComm*
Manuscript ID	CC-FEA-02-2025-001012.R1
Article Type:	Feature Article

ARTICLE

Interactions of CO and/or H_2O with mesoporous oxide-supported metal catalysts: the role of MSI effects

Received 00th January 20xx,
Accepted 00th January 20xx

DOI: 10.1039/x0xx00000x

Lingyiqian Luo,*[a] Ling Fei,[b] Rafel A. Hernandez,[b] and Hui Yan*[c]

Abstract

Mesoporous oxide-supported metal catalysts have been widely used in heterogeneous catalysis owing to their unique physicochemical properties such as uniform channels, tunable pore size, adjustable particle size, large pore volumes, big specific surface areas and tunable metal-support interaction (MSI). Carbon monoxide and water are the two gaseous species most seen in heterogeneous catalytic reactions including water-gas shift reaction, CO oxidation, and Fischer-Tropsch synthesis. Studying the interactions of CO and/or H_2O with mesoporous oxide supported metal catalysts will benefit in the rational design of efficient catalysts, with designed structures and better performance. This featured article focuses on the metal-support interactions that play a vital role in catalytic activity, by reviewing recent studies in literature and research from our group in the past five years. With the advance in various spectroscopic techniques such as Diffuse Reflectance Infrared Fourier Transform Spectroscopy (DRIFTS), Raman spectroscopy, and X-ray spectroscopy (XAS, XPS), one can better understand the interactions of CO and H_2O on mesoporous oxide-supported metal catalysts, MSI and its role in tuning catalytic activity.

1. Introduction

Carbon monoxide and water are the two most common reactants involved in a great amount of heterogeneous catalytic reactions, such as water-gas shift reaction, CO oxidation, Fischer-Tropsch synthesis, and so on. It is particularly important to study the interactions of CO and H_2O, individually or together with catalysts. In heterogeneous catalysis, active sites, coordination environment, geometric and electronic structures of a catalyst are critical factors that affect a catalyst's catalytic activity and selectivity[1,2]. Designing an efficient heterogeneous catalyst involves both proper control of the surface chemistry and rigorous control of the surface geometry of a catalyst at the micro-, meso- and macroscales. Mesoporous structure is defined as those porous materials with a pore size ranging between 2-50 nm. In the past decades, we have witnessed the progress of synthesis, characterization, functionalization, application of mesoporous materials since the discovery of M41S family (i.e., MCM-41, MCM-48, MCM-50, etc.) by Mobil researchers[3]. Ordered mesoporous materials (OMMs) represent a large group of materials including silicas, carbons, zeolites, metal oxides, organosilicas, metal- and covalent-organic frameworks[4]. These OMMs possess uniformity in size and regularly arranged mesopores, tunable pore sizes, large pore volumes, and high specific surface areas[4,5], which bring to an increased attention in fundamental research and industrial applications using OMMs, ranging from gas adsorption and separation, catalysis, sensors, to energy storage[4,6]. Several reviews about OMMs have been published recently. For example, Singh *et al.*[7] reviewed the metal nanoparticles supported on porous materials, with the focus on nanoporous metals and metal nanoparticles supported on metal-organic frameworks and zeolites. Gao *et al.*[8] reviewed the applications of metal and metal oxide supported on mesoporous carbon as catalysts in heterogeneous catalysis. Here, those topics are briefly mentioned, with more focus will be given to interactions of CO and/or H_2O with mesoporous oxide-supported metal catalysts and the role of MSI plays.

Based on the chemical composition, OMMs can be classified into silica-based and non-silica-based materials, and the latter can further be broken down to metal oxides and non-oxides materials (Figure 1). Generally, ordered mesoporous metal oxides (OMMOs) are formed relying on the interaction between surfactants and metal ions[9]. A recent development in the synthesis of mesoporous materials involved the cross-linking of various functional groups such as amines, strong acidic ionic liquids, sulfonates, triphenylphosphine, pyridine, and other similar species onto porous polymers[10]. OMMOs can be directly used as catalysts and have proven superior catalytic activity. Beyond that, they can be used as supports or doped with metals

[a] Currently at Department of Agricultural and Biological Engineering, Mississippi State University, Mississippi State, MS 39762, USA, E-mail: ll1339@msstate.edu.
[b] Department of Chemical Engineering, University of Louisiana at Lafayette, Lafayette, LA 70504, USA, E-mail: ling.fei@louisiana.edu; rafael.hernandez@louisiana.edu
[c] Department of Chemistry, University of Louisiana at Lafayette, Lafayette, LA 70504, USA, E-mail: hui.yan@louisiana.edu
* Corresponding author

to improve catalytic activity. The non-metal oxides such as mesoporous silicas and carbons are mostly treated as support or templates to obtain materials with desired mesoporous structures.

Compared with porous materials with single structures, hierarchically porous materials are characterized by multi-scale pores ranging from nanometer to millimeter[11]. Furthermore, hierarchical porous materials with mesoporous structures have attracted heated attention for various applications in catalysis, nanomedicine, and separation owing to their fascinating physical and chemical properties such as pore architectures and surface chemistry[12,13].

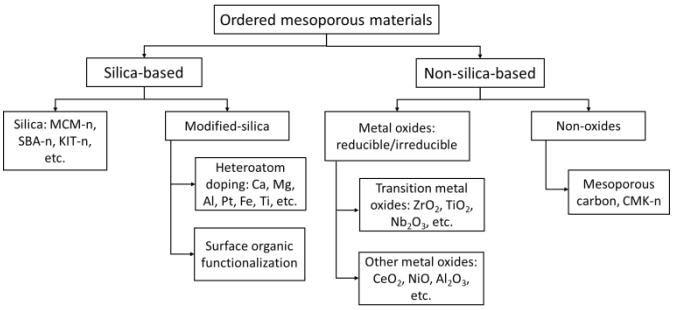

Figure 1. Types of common ordered mesoporous materials, modified from ref[14].

Mesoporous oxides-supported metal catalysts are of interest in heterogeneous catalysis because the metal-oxide interfaces have been considered as active sites, resulting in superior activity due to the strong metal-support interaction. Thus, understanding the dynamic interplay between the metal and its support is important to tune MSI and to improve the catalytic performance in heterogenous catalysis[15], and is considered a bridge between the design of supported catalysts and theoretical research on the atomic scale. MSI can further be categorized into strong/medium/weak metal-support interaction (SMSI, MMSI, WMSI), or covalent/electronic metal-support interaction (CMSI, EMSI). Changes to the support loading, morphology, metal loading, and surface modifications alter the interfacial perimeter and tune MSI[16]. Rapid development of many advanced characterization techniques such as X-ray absorption spectroscopy (XAS), X-ray photoelectron spectroscopy (XPS), diffuse reflectance infrared Fourier transform spectroscopy (DRIFTS) and Raman spectroscopy, has made it possible to investigate the MSI effects more accurately and comprehensively, and *in situ*[17–19]. In addition, combining molecular modeling and theoretical calculation, the MSI effects in a reaction can be better identified[17].

Hence, this feature article tends to demonstrate the role MSI plays in the interactions of water and CO with mesoporous oxide-supported metal catalysts within the past five years (2020-2025). Here, the article first introduces the types of mesoporous metal oxides and the supported metal catalysts, blended with the spectroscopic techniques used in investigating the physicochemical properties of the catalysts and their interactions, followed by a discussion of heterogeneous catalytic reactions over mesoporous oxide supported metal catalysts, with a focus on CO and water interactions over mesoporous oxide supported metal catalysts.

2. Types and synthesis of ordered mesoporous metal oxides

2.1 Ordered mesoporous metal oxides (OMMOs)

Mesoporous metal oxides (MMOs), especially transition metal oxides (TMOs), have risen promising applications in a wide range of fields including heterogeneous catalysts, sensors, and transparent high-power electronics[20], due to their structural uniformity, adjustable pore sizes, and large specific surface areas[21]. Meanwhile, there has been a breakthrough in studies of ordered mesoporous materials made of rare earth elements (i.e., cerium, lanthanum, etc.) [22,23]. Up to now, many commonly seen OMMOs such as Co_3O_4[24,25], TiO_2[26], Al_2O_3[27], ZrO_2[28], CeO_2[22], NiO[29], etc. have been successfully synthesized. Among non-silica mesoporous materials, mesoporous TMOs are especially important as they possess d-shell electrons confined to nanosized walls, redox active internal surfaces, and connected pore networks[29]. The OMMOs have better chemical activity, mechanical properties, and thermal stability than those of ordered mesoporous materials made with non-metal[9].

2.1.1 Single or mixed-OMMOs as catalysts

The simplest OMMOs are single metal oxides, denoted as M_1O_x, and can be categorized into non-reducible and/or reducible metal oxides. These metal oxides are inexpensive and readily available compared to precious metals[7]. Ceria (CeO_2) is a prominent material used as support or as catalyst. With its unique Ce^{3+}/Ce^{4+} redox property, it has been widely used in chemical and mechanical polishing, fuel cell oxidation catalysis, supercapacitors, and automotive exhaust treatment[30]. Like CeO_2, TiO_2 is also another reducible metal oxide used in such as WGS[17].

Mixed metal oxides, denoted as M_1O_x-M_2O_x, can act as catalysts in many heterogeneous catalytic reactions. For example, the NiO/CeO_2 catalyst has been studied for CO oxidation and proved to have high activity at low temperatures and satisfactory selectivity of CO_2 in the temperature range of 80-200 ^oC[31]. Ceria-silica mesoporous catalysts was studied for CO preferential oxidation (CO-PROX) in H_2-rich stream[32]. The addition of amorphous silica to ceria provided high dispersion and uniform distribution of ceria particles and their clusters of various sizes. The equimolar Ce:Si ratio demonstrated a better catalytic performance in CO-PROX, than that of Ce:Si = 4:1, due to its high ability to form anion vacancy and higher reducibility of ceria particles, confirmed by Raman spectroscopy and H_2-TPR. However, it is less common to directly use mixed oxides as catalysts without doping of active metal.

2.1.2 OMMOs as support for metal nanoparticles/nanoclusters

Oxide-supported metal nanoparticles/nanoclusters have indicated better catalytic activities compared to metal oxides alone, due to the bifunctional catalytic roles of the metal-oxide interfaces play in some reactions. More specifically, SMSI was first discovered by Tauster to describe the change of chemisorption properties for H_2 and CO over TiO_2-supported group 8 noble metals after high temperature H_2 or CO reduction[33,34]. The concept of EMSI has been proposed by Campell *et al*.[35] to characterize the chemical bonding and associated charge transfer at the interface between a metal and its support, both of which are able to tune the electronic and chemical properties of the sites on the metal particle's surface to improve the catalytic activity. Since this topic is broad and takes more thorough discussion, we focus on OMMO-supported metal nanoparticles/nanoclusters only, with a specific focus on the variety of mesoporous structures. OMMOs can act as inert supports to stabilize the incorporated metal nanoparticles. Single metal oxides with active metals (M_1/M_2O_x), and specifically, single metal doped to mixed oxides (M_1/M_2O_x-M_3O_y) have been found to enhance catalytic activity. A study by Lacoste *et al*.[36] investigated the CuO-CeO_2 catalysts supported on mesoporous silicas (i.e., SBA-15, SBA-16) with different morphologies (e.g., fibers and rods for SBA-15, and irregular shapes and spheres for SBA-16) and their effects on CO -PROX. Catalytic performance results showed that SBA-15 based catalysts, in the forms of fibers and rods and prepared by incipient wetness impregnation method, exhibited the best CO conversion, 98% and 84%, respectively. In addition, SBA-15 based catalysts showed better CO conversion and CO_2 selectivity than those of SBA-16 based catalysts, due to the interaction between gaseous reactants and the active phase facilitated by the cylindrical pores of SBA-15.

2.2 Preparation of OMMOs

The core of the strategy for synthesizing OMMOs is to "make holes" at the nanoscale, typically using templates. The rationale is that the metal precursor and template material cooperate with each other to form an ordered composite structure at a mesoscopic scale through interactive forces. The key factor of the template-assisted synthesis method is the "template", i.e., soft- or hard-templating method (Figures 2, 3), depending on the type of template materials used in synthesis.

2.2.1 Soft-templating method

The soft-templating method commonly makes use of materials with flexible nanostructures, including surfactants, flexible organic molecules, and block copolymers[37]. The interactions of these templates with precursors are through weak non-covalent bonding interactions, such as electrostatic, van der Waals interactions, and hydrogen bonding[37]. The surfactants used in the synthesis of OMMOs can be cationic, anionic, and/or nonionic. Copolymer, as an additive component of soft-templating method, has been used to functionalize mesoporous materials. For example, Ngo et al. applied a new approach for polymer functionalization of OMS by the co-condensation of silica precursor and a functional polymer bearing triethoxysilane end-group with a tailored poly (ethylene oxide)-*b*-polystyrene amphiphilic copolymer as pore template. The co-micellization of PEO-*b*-PS and functional polymer enables the incorporation of functional polymer into the mesoporous silica. Different ordered polymer-mesoporous silicas containing aryl, nitro or amide groups and high polymer content were synthesized[38].

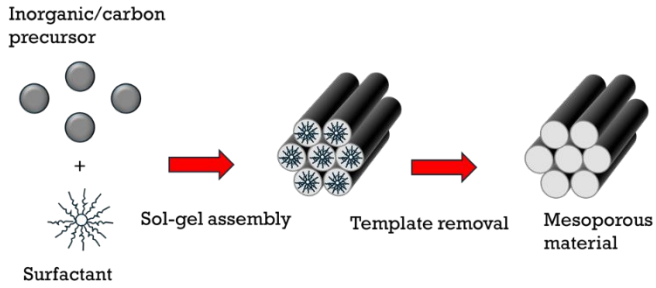

Figure 2. An example of schematic illustration of the soft-templating method of mesoporous oxides (hexagonal cylinder type, such as SBA-15).

2.2.2 Hard-templating method

Hard-templating method for OMMOs, in general, include four steps: (i) preparation of hard templates, (ii) impregnation of metal oxide precursor in the hard templates, (iii) conversion of metal oxide precursors to metal oxide framework, and (iv) removal of hard templates. Two common hard templates used in the synthesis of OMMOs are ordered mesoporous silicas and ordered mesoporous carbons.

Ordered mesoporous silica (OMS) itself can be fabricated through both soft-templating methods, with surfactant micelle as the SDA, and hard-templating methods without surfactants[5,38]. Furthermore, different types of mesoporous silica materials have been prepared by modifying the synthesis pathway and the type of surfactants. Those OMSs include but are not limited to Santa Barbara (SBA) series, Korean Advanced Institute of Science and Technology (KIT) series, Mobil Composition of Matter (MCM) series, Fudan University (FDU) series, Michigan State University (MSU), and Centrum voor Oppervlaktechemie en Katalyse (COK)[6,39,41–45]. OMSs have high thermal stability that can withstand high temperature and crystallize most of the metal oxides on the surfaces to obtain MMOs with high crystallinity, *via* the hard-templating method again. The advantage of using this method is that the final product of MMOs keeps the inverted mesoporous structure as the OMS hard template being used, seen in Figure 3.

Ordered mesoporous carbons (OMCs) are similar to the silica materials with many excellent properties such as relatively large specific surface area, large pore volume, well-ordered and controllable porous structure, excellent thermal and mechanical stability, and additional high electrical

conductivity[46,47]. Ryoo *et al*.[48] used mesoporous silica molecular sieve MCM-48 as template and sucrose as carbon source to synthesize ordered carbon molecular sieves, CMK-1, exhibiting Bragg diffraction of X-ray lines for the first time. OMCs are usually obtained by the replication of OMSs *via* a hard-templating method. MCM-48, SBA-1, SBA-15, SBA-16, KIT-6, and KIT-5 have been used as templates for the fabrication of OMCs (CMK-x) with different mesoporous structures[47]. OMCs can further be used as a hard template for the synthesis of other OMMs. Different from OMSs that use NaOH or HF to remove the template, the carbon template is mainly removed by calcination in air.

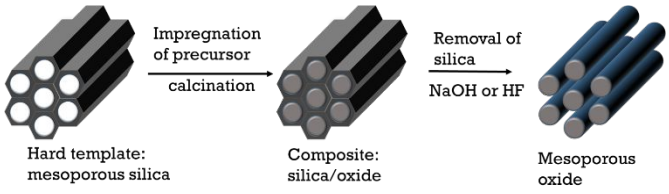

Figure 3. An example of schematic illustration of the hard-templating method of mesoporous oxides (hexagonal cylinder type, such as SBA-15 here).

2.2.3 Comparison of the soft- and hard-templating methods

The advantages of the soft-templating method include low-cost templates, simple synthesis process, and mild conditions for the process to be carried out. However, the main disadvantage is that the process is based on the sol-gel process, and the degrees of hydrolysis and polymerization of transition metal ions are difficult to control[20].

The hard-templating method has many advantages. The meso-structure of target materials can be controlled by selecting hard templates with desired structures. With the stability of mesoporous silicas at high temperatures, it allows many metal oxides to crystallize to obtain OMMOs with high crystalline walls. However, the hard-templating method also has some disadvantages. First, the targeting mesoporous metal oxides need to be stable in NaOH or HF solutions during the removal of the hard templates. Second, a solution step is involved in the process of introducing the transition metal precursor, which limits the selection of the materials. In terms of using OMC as a hard template, the major disadvantage is its poor wetting ability of the pore walls with the aqueous precursor solution[20,49]. In addition, the stability of hard templates under reaction conditions, such as water and heat, needs to be considered. For example, SBA-15 and MCM-41 are debatably stable in water, under hydrothermal treatment or under high energy e-beam during characterization[50,51]. SBA-15 is considered to be more stable than MCM-41 due to its thicker wall[51], and a low hydrothermal stability in hot water and aqueous solutions is more obvious for MCM-41 than SBA-15[52,53].

2.2.4 Mesoporous alumina as an example

Since the rapid development of OMS, the progress of mesoporous materials has been extended to non-silica oxides such as TiO_2, CeO_2, ZrO_2 and Al_2O_3 etc. [30,54–56], to alleviate the coking and deactivation of catalysts, originated from the clogging of traditional microporous catalysts. As a representative, mesoporous alumina (MA) has been extensively used. Alumina exists in various crystalline phases such as α, γ, η, and δ. Among them, γ-Al_2O_3 has a large surface area and a crystalline structure, which has been considered as an important support in automotive and petroleum industries[57]. The catalytic performance of MA-supported catalysts strongly depends on the textural properties of the alumina supports. Vaudry *et al*.[58] were the first group prepared mesoporous alumina using long-chain carboxylic acids, as previous alumina materials prepared via soft templates using surfactants did not show long-chain order. The group has developed several methods that involve cationic, anionic, and neutral routes. Among these synthesis routes, the anionic route using SDAs such as lauric and stearic acids would provide the largest surface area (500-700 m^2/g). A unique mesoporous–macroporous spherical γ-Al_2O_3 (γ-Al_2O_3 -CD) with a reduced amount of surface hydroxyl groups has been successfully synthesized by using dodecane and hydrophilic-modified activated carbon as dual-template agents[59]. The mercury intrusion porosimetry (MIP) specific surface area is measured to be 256 $m^2 \cdot g^{-1}$ and a pore volume of 0.62 $mL \cdot g^{-1}$, compared to those of 204 $m^2 \cdot g^{-1}$ and a pore volume of 0.40 $mL \cdot g^{-1}$ of untreated γ-Al_2O_3. γ-Al_2O_3 -CD was stable since its MIP specific surface area remained virtually unchanged at 255 $m^2 \cdot g^{-1}$ after a 120 hr hydrothermal treatment in a tube furnace under water steam at 600 °C.

3. Applications of OMMO supported metal catalysts in reactions involving CO and H_2O

The most common oxide-supported metal catalysts are categorized into (1) monometallic catalysts supported on single metal oxides, in the form of M_1/M_2O_x, where M_1 refers to active metal and is mostly noble metals. This group of catalysts can be further promoted by adding one or more active metal(s) as additives, in the forms of M_1-M_2/M_3O_x, M_1-M_2-M_3/M_4O_x etc.; (2) monometallic catalysts supported on mixed metal oxides, M_1/M_2O_x-M_3O_y. Typical metal-support phenomena is related to charge transfer, the interfacial perimeter, metal nanoparticle morphology, chemical composition and MSI[60]. A catalyst is usually treated in the H_2-rich environment as it creates a strong interaction between the metal and support[61,62], which can prevent the sintering of metal. Table 1 summarized some common mesoporous catalysts used in various heterogeneous catalytic reactions in the past five years, listed with reported catalytic activity test and spectroscopic techniques other than TPR and reactor studies. Since all reactions involve CO, CO conversion (X_{CO}) or temperature at 100% CO conversion (T_{100}), is considered the intuitive parameters to determine the catalytic performance and are listed in Table 1.

Table 1. Common mesoporous catalysts for various heterogeneous catalytic reactions from 2020-2025

Reaction	Active metals (type)	Supports (type)	X_{CO} (%) or T_{100}[a]	Spectroscopic techniques	Ref
WGS	Ni (mono-) Ni/Ce (bi-) Ni/Zr Ni/Zr-Ce (tri-) @400°C[b]	SBA-15	95.5 94.7 94.6 98.1	*In situ* DRIFT XPS, XAS	63
	Cr/Fe (bi-) S60/Cr/Fe[c] @450°C	SBA-15	10 70	*In situ* FTIR	64
	xNi-yCu (bi-)[d] @450°C	CeO_2 Al_2O_3 Mn_2O_3 CeO_2-Al_2O_3 CeO_2-Mn_2O_3 Al_2O_3-Mn_2O_3	68 74 64 70 75 85	-	65
	xPtSmCoO$_3$ Pt (0) Pt (0.37) Pt (0.83) Pt (0.88) @400 °C	SBA-15/GO	10 78 95 82	*In situ* DRIFT	66
CO oxidation	2 nm Pt NP 4.8 nm Pt NP	m-Co_3O_4[e]	160°C 190°C	AP-XPS, *in situ* DRIFT	67
	2.9 nm CeO_2-Pd NP 3.8 nm CeO_2-Pd NP ZrO_2-Pd	SBA-15	75°C 90°C 225°C	*In situ* DRIFT XPS	68
	Pt Pt Pt	MCM-41 Al-modified MCM-41 (Si/Al=30) Al-modified MCM-41 (Si/Al=60)	240°C 210°C 160°C	*In situ* DRIFT	69
	1% Pt_7Ni_3 (0.7%Pt)	dendritic mesoporous silica (KCC-1)	100°C	*In situ* DRIFT	70
	Co_3O_4	crystalline mesoporous Ta_2O_5	130°C	*In situ* DRIFT XPS	71
	Rh, Ru, Ir, Pd and Pt	hierarchical meso- and macroporous structure mesoporous	100°C 115°C	*In situ* TEM, XPS	72
Fischer-Tropsch synthesis	Co-KCuFe Ni-KCuFe Mg-KCuFe Mn-KCuFe KCuFe @270 °C	m-Al_2O_3	93 77 93 95 94	XPS, XAS/XANES	73
	Sn(0 wt.%) Sn(0.25 wt.%) Sn(0.65 wt.%) Sn(1.82 wt.%) @230°C	m-Co_3O_4-Al_2O_3	81.5; *99.6@ 255°C,* 79.1 65.5 52.7	XPS	74
	Co CoRu CoFe	MCM-41	64 77	FTIR, XPS	75

	CoNi @240°C		65.5@ 210°C 72		
	Ni	FSCe Ce/KCC-1 KCC-1	95.67 58 50	Raman, FTIR XPS	[76]

a: T_{100} is the temperature at 100% CO conversion. b: only temperature was listed for CO conversion for direct comparison within the group, refer to the cited literature for detailed experimental condition; c: S60 stands for Span 60 ($C_{24}H_{46}O_6$), a surfactant; d: x (1-10%), y (5-12.5%) represents various metal loadings; e: m stands for mesoporous

3.1 Water-gas shift reaction on OMMOs supported metal catalysts

The water-gas shift reaction (WGS, Eq. 1) is a typical heterogeneous reaction that contains both carbon monoxide and water as reactants. It has a wide range of applications in the manufacture of ammonia, hydrogen, and methanol[64,77,78].

$$CO + H_2O \rightarrow CO_2 + H_2 \quad \text{(Eq. 1)}$$

On a metal supported on metal oxide catalyst, it is generally accepted that the metals actively adsorb CO and the oxides serve as supports to activate H_2O. Therefore, selecting an active metal incorporated on desired metal oxides, as a catalyst, will help promote the reaction. Oxygen mobility of a reducible oxide supports causes the reduction of the metal oxides and creates oxygen vacancies, which is considered a key step in WGS reaction mechanism to improve its activity. Some studies also considered that active sites locate at the metal-support interfaces of a catalyst because those interfaces can perform the dual function, which are the dissociation of H_2O and the reaction with CO[79]. Two prominent reaction mechanisms have been proposed for WGS: (1) associative mechanism, where CO adsorbs on the metallic site and form either formate or carboxyl intermediates with the OH- dissociated from water; (2) redox mechanism, where CO adsorbs on the metallic site then reacts with lattice oxygen to form CO_2, while H_2O adsorbs and dissociates on the support sites to re-oxidize the supports and produce H_2. Hence, studying interaction of CO with metal nanoparticles and interaction of water with mesoporous metal oxides are important in understanding the MSI while designing efficient catalysts.

3.1.1 Interaction of CO with metal nanoparticles

In situ and *operando* spectroscopy is a set of powerful tools to analyze the nature of catalysts, especially for investigating adsorbates on the surface during the process of a reaction[2]. Infrared (IR) spectroscopy is one of the most common spectroscopic techniques applied to the characterization of catalysts and to study detailed interactions of reactants and adsorbed species on the catalyst surfaces under *operando* conditions[80]. During WGS reaction, CO molecules strongly adsorb on metal nanoparticles, which can be observed by *in situ* DRIFTS. Typical IR peaks include gaseous CO, various modes of CO adsorb on active metal with different coordination numbers, denoted as M-CO, and CO_2 in gas phase. *In situ* CO-DRIFTS has been used as a method to investigate the oxidation state, local geometric structure, and coordination environment of oxide-supported metal catalysts[2]. Our group[54] applied CO as a probe molecule to study pore structure of 1% Pt supported on various ordered mesoporous CeO_2, synthesized from hard-templating method using SBA-15, KIT-6 and COK-19, and template-free SiO_2 via *in situ* DRIFTS (Figure 4). The study was able to identify several Pt-CO_{ads} species on various structured mesoporous Pt-CeO_2. The types of Pt-CO_{ads} species are identical for all synthesized mesoporous Pt-CeO_2 and are independent of the pore morphology, including an intense band at assigned to CO-Pt^0 or CO-$Pt^{\delta+}$ (2096 cm^{-1}); and CO linearly adsorbed on defect sites, i.e. steps/corners and terraces (2079 cm^{-1} and 2062/2059 cm^{-1}). Information of the active metal sites have been deduced based on the integrated area in 2150-1750 cm^{-1} region in their respective IR spectra. The results showed that the CeO_2-supported Pt catalyst synthesized using SBA-15 obtained the largest integrated area of the Pt-CO_{ads} region, which is an indicator of the greater number of Pt active sites as well as the strongest CO adsorption behavior. These can be attributed to the catalyst's (from SBA-15) largest pore volume and pore size. The morphological effects are more obvious on the carbonate/formate regions of DRIFT spectra from 1700–1000 cm^{-1}. The catalyst made by the SBA-15 template accumulated less carbonate species on the catalyst surface and resulted in a better performance than the catalysts made by KIT-6 and COK-19 templates, and the template-free ones. Our results provided a fundamental understanding of pore morphology on ordered mesoporous CeO_2-supported Pt catalysts with the interaction of CO and will help further investigation of the reaction mechanisms involving CO.

3.1.2 Interaction of H_2O with nanoparticles on OMMOs

The role of water/moisture has received increasing attention, not only because of its wide existence in most chemical reactions either in the form of solvent, impurity, reactant, intermediate, or product but also because of its exceptional promotional or inhibiting effects on catalytical reactions. It's been agreed that H_2O exists in both molecular and dissociative forms during the WGS reaction. Dissociation of water is a critical step in catalytic reactions on reducible oxide-supported metal catalysts, and can be affected by the nature of support, metals, and metal-support interfaces. Hydroxyl forms on metal surfaces, through partial dissociation of an adsorbed water molecule to form a surface hydroxyl (*OH) and an adsorbed hydrogen atom (*H). Taking ceria as an example, the adsorption energy for a molecular H_2O is 0.4 eV smaller than its dissociative adsorption energy on CeO_2 (111)[81]. Since ceria has strong redox property, water adsorbs on reduced ceria is suggested to oxidize ceria and produce hydrogen. For water interaction over

the mesoporous oxide-supported metal catalysts, *in situ* DRIFTS is useful in determining the hydroxyl stretching bands associated with molecular and dissociative water molecule, and hydrogen bonding[81]. Our group[81] applied *in situ* DRIFTS to identify vibrational OH bands on mesoporous ceria surfaces during their interaction with water. Water on mesoporous CeO_2 surface showed six hydroxyl (OH) stretching bands, including configurations such as dangling or mono-coordinated Ce-OH on highly defected surfaces, on unsaturated Ce sites or defect sites (Ce^{3+}). And the surface hydroxyl groups formed hydrogen bonds, resulting in a red shift in the IR bands. The H/D isotope exchange method was used to explore the reaction mechanisms and OH was found to be successful in exchange with OD bands.

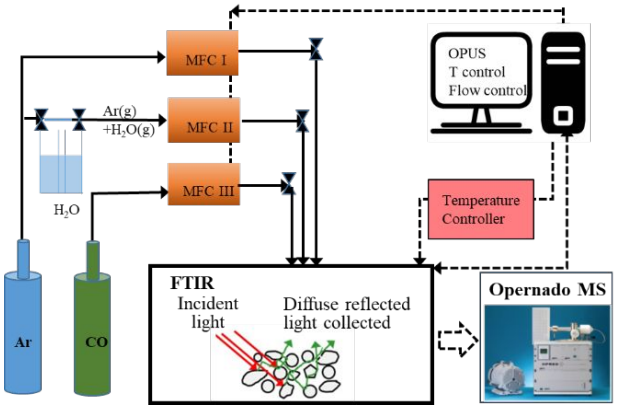

Figure 4. *In situ* variable-temperature DRIFT-MS system in our group.

3.1.3 Impact of the MSI effects on catalytic activity

The primary role of a support in catalytic reaction is to stabilize the metal nanoparticles *via* anchoring[82]. Electron transfer takes place due to EMSI[83]. Investigating the interaction between metals and supports (MSI) is important as the active sites of a supported catalyst are typically located at the metal-support interfaces. This is made to be possible by rapid development of advanced characterization techniques such as X-ray absorption fine structure (XAFS), ambient-pressure X-ray photoelectron spectroscopy (AP-XPS), diffuse reflectance infrared Fourier transform spectroscopy (DRIFTS) and Raman spectroscopy. For example, our group has used *in situ* and variable temperature DRIFTS (VT-DRIFT) to characterize Pt-mesoporous ceria made from several hard templates and to study their interaction with CO and H_2O[54,81].

Numerous studies have attempted to investigate the WGS catalytic activity over oxide-supported metal catalysts, which are categorized into high-temperature shift (HTS) catalysts and low-temperature shift (LTS) catalysts. Studies suggest that preparation of the oxide-supported metal catalysts using ordered mesoporous silica support helped to improve the catalytic performance. For example, Carta *et al.*[84] prepared a single-step nanocomposite catalyst by depositing and impregnating Pt-CeO_2 nanophases on an ordered mesoporous silica support SBA-16 for WGS reaction. The research indicated that the key to active and stable catalysts was the confinement of the active phase within the SBA-16 scaffold, and the enhancement of the interaction between Pt nanoparticles and CeO_2 nanocrystallites. The deactivation of the Pt catalyst is shadowed by the H/Pt value measure by H_2 chemisorption. The study pointed out that the decrease of activity of Pt to H_2 could be caused by several phenomena such as partial sintering, occlusion of Pt nanoparticles by the support and by some extent of electronic SMSI. Similarly, our group[54] compared CO interaction with various mesoporous Pt-CeO_2, synthesized using mesoporous silica templates SBA-15, KIT-6, and COK-19. The surfaces with CO were characterized by *in situ* DRIFTS, which demonstrated an obvious increase in intensity and then disappearance of a representative peak at 1389 cm^{-1} from 150°C to 250°C, corresponding to ν_s(OCO) of bridged carbonate on Pt-CeO_2, which was not observed for m-CeO_2, independent of the type of silica templates. This observation indicated that there was a dynamic change of active sites at the interfaces of metal-support when temperature changes, which in turn affected the products, possibly from a new site originating from the SMSI, compared to the mesoporous CeO_2 supports.

For a newly developed PtSSG (x$PtSmCoO_3$/SBA-15/GO, Pt loadings x were 0.37, 0.83 and 0.88) mesoporous material[66], the active metal Pt was found to present both as single atoms and nanoparticles over PtSSG samples. Graphene oxide (GO) acted as an electron transfer bridge and strengthened the metal-support interaction between Pt and SSG, thus enhancing its catalytic activity towards WGS. The lower Pt-loading produced single atom $Pt_{0.37}$SSG, which had the highest specific rate (0.84 mol_{CO} /g_{Pt}) and TOF (4.5 $\times 10^{-2}$ s^{-1} at 250 °C), due to the higher oxidation state of Pt species (3.39) via Co-PtOx, higher O_{ads}/O_{lat} molar ratio and better low-temperature reducibility. CO_2 was detected by DRIFTS from the redox reaction between CO and oxygen species over single atom $Pt_{0.37}$SSG catalyst, while formate or carboxylate intermediates formed over the $Pt_{0.88}$SSG sample through CO reacted with OH by associative mechanism.

Even though MSI is closely related to catalytic activity, it should be noted that stronger MSI does not necessarily mean higher activity. Therefore, rational tuning of MSI to obtain the appropriate adsorption strength to the reactants is proposed for the design of catalyst. Zhang and co-workers[85] reported an effective strategy to modulate the interfacial interaction of Co/CeO_2 catalysts by treating the CeO_2 support with NH_3. This treatment not only weakened the MSI between Co, Fe, Ni and the CeO_2 support to strengthen CO adsorption and activation ability, but also generated more oxygen vacancy under reaction conditions to accelerate H_2O activation. Gao *et al.*[86] indicated that medium MSI and EMSI occurred between Pt nanoclusters (NCs) and mesoporous titania (mp-TiO_2) support, reflected by the well encapsulation of Pt NCs by mp-TiO_2. The self-enhancing activity was discovered in Pt-mp-TiO_2, a highly stable supported metal cluster catalyst, which played an important role in WGS activity, given a 95% CO conversion rate and long-term stability.

3.2 CO oxidation on OMMOs supported metal catalysts

CO oxidation (Eq. 2) is another important heterogeneous reaction that has drawn great attention due to its wide applications in the control of automotive emission and CO preferential oxidation (CO-PROX) for proton exchange membrane fuel cell[2,19]. For example, owing to the effect of CO poisoning in fuel cell, excess H_2 is preferred in CO-PROX[31]. CO adsorption is frequently used to identify oxidation states and coordination numbers of metal active sites on surfaces of catalysts. Superior catalysts for low-temperature CO oxidation are generally noble metals (Au, Pt, Pd, etc.) supported on mesoporous reducible oxides (m-CeO_2, m-TiO_2, m-ZrO_2, etc.). Among these catalysts, early research showed Au-based catalysts exhibited excellent activity at temperatures lower than 100 °C while Pd-and Pt-based catalysts possessed high CO conversion (100%) at temperatures higher than 100 °C[70]. O_2 activation is the key step at the metal-oxide interface to improve catalytic performance.

$$2CO + O_2 \rightarrow 2CO_2 \qquad \text{(Eq. 2)}$$

In the catalysts doped with platinum group metal (PGM), Pt has received much attention because of its intrinsically high activity for CO oxidation, although Pt is a rare earth metal that exists at a concentration of only 0.005 ppm in Earth's crust. The adsorption of CO on Pt sites is too strong and exclusive, leaving O_2 with no extra active sites for activation at low temperatures. As temperature increases, O_2 adsorption and activation occur, and the reaction rate of CO oxidation increases[87]. The adsorption behavior of CO over Pt catalysts has been reviewed by Dey *et al.* [87] and is only briefly described here. The support usually has effects on dispersion and oxidation state of Pt active sites. The most active phase in CO oxidation is metallic Pt and it exists on fresh catalysts, while PtO and Pt^0 coexist on the spent catalysts.

3.2.1 Promotional role of water in CO oxidation

Moisture has inevitably existed in practical applications and thus it is important to study catalytic activity with the presence of moisture.[88] H_2O plays two possible roles in CO oxidation. First, it can promote the reaction by activating molecular oxygen on the catalyst surface. Second, water assists in decomposing carbonates (CO_3^{2-}) that may form on the catalyst surface to accommodate additional reactants on the surface during the reaction.

Li *et al*[89] studied the catalytic behavior of mesoporous Pd/CeO_2 under moisture condition. The result indicated that when 2.5 vol.% of H_2O was introduced to the feed gas, the catalytic activity significantly enhanced, as the CO total conversion (100%) temperature decreased from 40 °C to 30 °C, the TOF value increased from 23.60 × 10^{-3} s^{-1} to 38.48 × 10^{-3} s^{-1} correspondingly. The presence of molecular water promoted the CO oxidation due to the lower activation energy, 10.8 kJ mol^{-1} under moisture condition, versus the 51.7 kJ mol^{-1} under dry condition.

However, whether water promotes CO oxidation depends on the type of support. A recent study, combined experimental with theoretical studies, discovered a water promoted [90] Mars—van Krevelen reaction mechanism dominated low-temperature CO oxidation over Au-Fe_2O_3, but not over Au-TiO_2. For Pd supported on SnO_2, TiO_2, and SiO_2, PdO/SnO_2 demonstrated increased activity in the presence of water vapor while PdO/SiO_2 experienced minimal effects and water poisons PdO/TiO_2[91]. Water vapor showed differential impacts on the catalytic performance of these catalysts by changing the energy barriers associated with the CO oxidation. On PdO/TiO_2, the presence of H_2O or H–OH increased the energy barrier for CO to abstract surface oxygen, thereby diminishing catalyst activity under humid conditions and gradually leading to deactivation due to accumulated surface H_2O and OH species. Conversely, on PdO/SnO_2, the energy barrier reduced to increase CO oxidation activity, due to the beneficial effects of surface OH groups dissociated from H_2O[91].

3.2.2 The role of MSI in CO oxidation

Mesoporous metal oxides used to be considered acting as support at the perimeter of the catalyst surface to stabilize the incorporated metal nanoparticles. However, this concept has changed over the years since the small metal nanoparticles that adhered to supporting oxides exhibited remarkable performance for many applications[92]. It's agreed that the highest activity occurred at the interface between certain metals and oxides, where the interaction between a metal and oxide support via SMSI greatly affects the properties of the supported metal, such as metal dispersion, size distribution, valence state, and thermal stability, which in turn alters the catalytic activity of the catalyst[93]. In CO oxidation, the loaded metal on the support acts as a chemisorption site for CO and forms an interface with the support to provide a site at which the reaction is easier to occur.

In addition, CO catalytic activity is associated with sizes of active metal nanoparticles. Studies by Kim *et al.*[67] and Murthy *et al.*[68] indicated that catalysts with smaller NPs are more active than the larger ones in the catalytic CO oxidation. This is due to the higher concentration of active sites on the small NPs, which effectively increases/improves the metal-oxide interface, hence boosting the oxidation reaction.

Other than the type of dopant metals (Au, Pt, Pd etc.), which controls the strength of MSI, varying metal loading has been proved to be an effective method to improve the performance of CO oxidation. For example, the rate of CO oxidation is higher with rising Cu content from 0.06 wt. % to 0.86 wt. % at 120, 180, and 250 °C, owing to a higher concentration of Cu single atoms from 0.06 wt.% loadings than 0.86 wt. % [94]. The calculated TOF value, for CO oxidation on the catalyst CeO_2—TiO_2 loaded with 0.06 wt.% Cu, is 4.0 × 10^{-2} s^{-1} at 250 °C, which is about two times higher than that of the highly active Cu/UiO-66 catalyst with Cu single sites in a Zr-based metal–organic framework material (TOF = 1.8 × 10^{-2} s^{-1})[94]. It clearly demonstrated that

nanoparticles with mesoporous transition metal oxides at the interface significantly enhanced the rate of the oxidation of CO. Thus, understanding the interaction between metal nanoparticles and mesoporous metal oxides is crucial for developing mesoporous oxides supported metal catalysts with desired physicochemical properties and applications. The same metal can act very differently, depending upon its interaction with the type of support and their structures.

Raman spectroscopy can provide molecular and structural information on species, especially for those that are located at low wavenumber and are difficult to detect by traditional methods. Therefore, it is a promising technique for *in situ* characterization of active oxygen vacancies. Compared to normal Raman spectroscopy, surface-enhanced Raman spectroscopy (SERS) has higher sensitivity even at the single-molecule level, showing great potential in *in situ* catalytic studies. However, plasmonic metals are only limited to Au, Ag, and Cu nanomaterials with specific structures, which inhibit the applications of *in situ* SERS on other metal and/or oxide surfaces during catalytic reactions. Wei *et al*.[55] studied the CO oxidation over Pt-CeO_2 catalyst. And to achieve *in situ* Raman investigation at Pt-CeO_2 interface, plasmonic metal Au core@Pt shell-CeO_2 satellites nanostructure was designed. Direct *in situ* Raman spectra along with isotopic measurements demonstrated that the existence of Pt-CeO_2 interfaces can promote the CO oxidation activity, from the efficient activation of oxygen at the interfacial Ce^{3+} defect sites to chemisorbed Pt-O and lattice Ce-O sites. Time resolved *in situ* SERS results showed that the chemisorbed Pt-O species were more active than the lattice Ce-O species and preferably react with adsorbed CO.

Grabchenko *et al.*[95] studied the role of SMSI in CO oxidation over mesoporous Ag/CeO_2 catalysts prepared by different methods. In this study, the authors used Raman and XPS techniques to study the lattice oxygen defects and the surface of the catalysts. Raman spectra indicated that the catalysts prepared by the co-deposition precipitation (co-DP) and impregnation of the reduced CeO_2 (red-imp) methods were found to have increased amount of oxygen vacancies, which was the result of strengthening of MSI. And the strength of the MSI in the following order for the catalysts Ag/CeO_2: Ag/CeO_2 (imp) < Ag-CeO_2 (co-DP) ≤ Ag/CeO_2 (red-imp) directly correlates to the increase of CO oxidation activity.

AP-XPS is used to evaluate the chemical states and surface composition of catalysts. Qualitatively, binding energy is a measure of how tight an electron is bound to an atom. Kim *et al.*[67] applied *operando* AP-XPS under CO oxidation conditions (0.4 mbar CO and 1mbar O_2) to understand the catalytic enhancement behavior at the Pt/m-Co_3O_4 surface (*m* stands for mesoporous) by studying the SMSI effect at the interface of Pt and Co_3O_4. The study compared the binding energies of the Pt nanoparticles with different particle sizes (i.e., 2 nm Pt/m-Co_3O_4 and 4.8 nm Pt/m-Co_3O_4) and showed that Pt 4f/Co 3p ratio decreased for both catalysts, from 0.63 to 0.46, and from 0.41 to 0.36, respectively. And the smaller Pt 4f/Co 3p ratio of the 4.8 nm Pt/m-Co_3O_4 is due to the difference in Pt nanoparticle (NP) dispersion. On the other hand, the smaller 2 nm Pt NP dispersed more effectively on the Co_3O_4 support, creating a larger Pt concentration at the interface. The relatively small decrease of the Pt 4f/Co 3p ratio for 4.8 nm Pt/m-Co_3O_4 also indicated that the metal encapsulation of 4.8 nm Pt NP was less drastic compared to that of 2 nm Pt NP.

When MSI is too strong, it will suppress the CO oxidation activity and change the reaction pathway. A recent study of CO oxidation on Pd supported on mesoporous Fe_2O_3 [96]shows that the catalyst followed the Pd/Fe dual-site mechanism instead of the classical Mars–van Krevelen mechanism. Its catalytic activity was seriously suppressed because of the excessive encapsulation of the active Pd sites by FeOx overlayers.

3.2.3 Newly developed catalysts with mixed metals or mixed oxides

Bimetallic cluster supported on mesoporous materials will take advantage of both MSI and synergistic effect of both metals, to enhance CO oxidation performance. A high-surface area dendritic mesoporous silica (KCC-1) was used as a support to confine Pt–Ni bimetallic nanoparticles (NPs), and then was used as the catalyst for the CO oxidation. Compared with 1% Pt/KCC-1 and 1% Ni/KCC-1, the 1% Pt_7Ni_3/KCC-1 bimetallic catalyst demonstrated a substantial improvement in the CO oxidation activity (Table 1, T_{100} is 100°C) [70]. This is supported by a lower E_a at 52.0 kJ mol^{-1} of 1% Pt_7Ni_3/KCC-1 compared to those of 1% Ni/KCC-1 and 1% Pt/ KCC-1 catalysts at 67.5 and 79.5 kJ mol^{-1}, respectively. The superior CO oxidation performance of 1% Pt_7Ni_3/KCC-1 was attributed to the support effect of KCC-1, and the synergetic effect between Pt and Ni, because the large specific surface area and abundant pore structure of KCC-1 facilitate the high dispersion and enhance the thermal stability of Pt—Ni bimetallic nanoparticles due to the confinement effect.

Recent developed High Entropy Alloy (HEA)-based nanocrystals, made of five platinum group metals (Rh, Ru, Ir, Pd and Pt), with hierarchical meso- and macroporous and ordered mesoporous structures, showed enhanced activity for CO oxidation and higher chemical stability, compared to nonporous particles with the same chemical composition as reference. T_{100} was found at 100 °C for the hierarchical meso- and macroporous particles and 115 °C for the mesoporous particles[72].

The combination of mesoporous with other structured materials also will improve the performance of CO oxidation. The temperature of 90% CO conversion rate of Co_3O_4 on crystalline mesoporous Ta_2O_5 is approximately 130 °C, compared to using amorphous, mesoporous and crystalline Co_3O_4 as supports at temperature higher than 150 °C[71].

3.3 Fischer-Tropsch synthesis on OMMOs supported metal catalysts

The Fischer-Tropsch synthesis (FT, Eq. 3) process is a mature technology that aims at converting syngas to liquid fuels, such as olefins, paraffins, alcohols, and aldehydes.

$$n\ CO + (2n + 1)\ H_2 \rightarrow C_nH_{2n+2} + n\ H_2O \qquad \text{(Eq. 3)}$$

The FT process is ideally conducted at 200-300 °C and at 1.01-6.06 MPa for high selectivity in liquid products. However, many factors such as the type of catalysts and supports, the preparation methods, reaction conditions (i.e., syngas composition, temperature and pressure, residence time of the feed in the reactor) control FT activity, the syngas conversion and hydrocarbon selectivity.

3.3.1 Effects of water on the FT synthesis

Water is the most unwanted by-product in the FT process. Dalai *et al.*[97] reviewed the effects of water on the performance of various Co-based catalysts for the FT synthesis, including SiO_2-, Al_2O_3-, TiO_2-supported Co catalysts. The study indicated that water vapor had a significant effect on the reduction behavior of various Co-supported catalysts, and added water vapor had a positive effect on unsupported Co_3O_4 catalyst. The addition of water in FT synthesis decreases or increases CO conversion, and affects selectivity of methane, C_{5+} hydrocarbons, olefins and CO_2 depending on the Co loading, supports, promoters, and the process conditions. When comparing these three supports, water effects are positive and result in higher CO conversion for Co-based catalysts on SiO_2, whereas for Co-based catalysts on Al_2O_3, the effects are negative. For Co-based catalysts on TiO_2, water has little or no impact on CO conversion.

However, too much water will result in a competition of WGS with FT reaction. A catalyst with a composition of 25 wt.% Co, 3 wt.% Mn and 0.5 wt.% Pt exhibited a CO conversion at a rate of 1.75 molCO.molCo^{-1}.h^{-1}, a 73% C_{5+} selectivity, and less than 5% methane formation in aqueous phase FT synthesis[98]. The addition of Pt and Mn significantly improved the reducibility of cobalt-oxide, enhanced the Lewis-acid base interaction between O atom of CO and Mn^{2+} at the interface of Co-MnO sites, and strengthened CO adsorption to improve the catalytic activity. Although high H_2O partial pressure and H_2/CO ratios resulted in enhanced methanation and WGS activities, CO conversion rates were modeled well by FT empirical rate laws with little H_2O term dependence. Thermodynamic data favored the FT products over the WGS reaction, while CoO particles favored the WGS reaction that produces CO_2 and H_2, followed by the formation of CH_4 and lower hydrocarbons.

3.3.2 Strong metal-support interaction on FT synthesis

Types of support have a significant effect on the rate of CO conversion and stability of catalysts during the FT process. Platero *et al.*[99] prepared a series of Co supported on mesostructured TiO_2 catalysts by varying the calcination temperature. The mesoporous Co/TiO_2 catalyst showed a better catalytic performance when the support was treated at 380 °C because the mesostructured TiO_2 served as metal nanoparticle confinement. The SMSI has been hindered on the commercial P90 TiO_2 support due to the lack of confinement by the mesoporous structure. The calcination temperature in the synthesis process affected the SMSI as it caused the confinement of the reduced Co species to form homogeneous distribution of Co, resulting in hinderance of the SMSI for the support.

To investigate the promoting effect of a second metal on the FT synthesis, Mohammed *et al.*[65] added Fe, Ru, and Ni to Co-MCM-41 and carried out CO conversion activity study in a three-dimensional printed microreactor. In terms of CO conversion, Ru exhibited synergistic behavior in bimetallic CoRu-MCM-41 and showed the highest conversion rate of 77.4% at 240 °C. More significantly, the second metal other than Co, such as Fe, Ru, and Ni, was unambiguously promoting the selectivity of hydrocarbons and CO conversion. The reaction temperature also affected the CO conversion rate. The presence of Ni did not favor the formation of propane and butane, as it produced methane exclusively at temperatures greater than 210 °C, while both Ru and Fe showed a positive effect with CoFe-MCM-41 having the highest hydrocarbon selectivity. In the temperature range of 240–300 °C, the CoFe bimetallic catalyst showed selectivity of propane and butane at 39% and 8%, respectively. On the other hand, the CoRu catalyst showed selectivity of propane and butane of 33.5% and 11.2%, respectively. In addition, the CoFe catalyst showed much higher stability than the other bimetallic catalysts, following the order of CoFe-MCM-41 > Co-MCM-41 > CoNi-MCM-41 > CoRu-MCM-41. To investigate the effects of MSI, catalyst morphology, and mesoporous SiO_2-structure on the kinetics of the FT reaction, three different types of mesoporous silica (i.e., MCM-41, SBA-15, and KIT-6) supported on Co-Ru bimetallic nanocatalysts were prepared by the same group. According to their results, types of mesoporous silica support significantly affected the FT kinetics and stability of metal catalysts. Based on the results of CO conversion, the ability of the catalysts to withstand the FT deactivation rate followed the order of CoRu-KIT-6 > CoRu-MCM-41 > CoRu-SBA-15. And this study further indicates that even though the support is of the same chemical formula, the meso-structure still plays a pivotal role in the catalytic performance[100].

MSI will affect the selectivity of side reactions to generated other products such as alcohol. MSI can be tuned by pore size to adjust the high alcohol percentage. For example, a double-layer MoS_2 stacking (~31.2%) supported on Mg-modified mesoporous silica KNiMoS/Mg-MS-20, with dominant and proper slab length, showed the highest alcohol selectivity of 66.3%, C_{2+}OH selectivity of 80.5% in the alcohol[101]. It was noted that the proportion of ethanol and propyl alcohol increases with decreasing pore size, suggesting that the MSI between Mo and the support could be tuned to induce a higher sulfidation degree of Mo species and a higher proportion of NiMoS species, thus enhanced selectivity in high alcohols.

A nickel supported on fibrous silica mesoporous ceria (Ni/FSCe), with cockscomb-like structure, took advantage of the synergistic effect of high amount of inter-nanoparticle oxygen vacancies (high basicity) and well-dispersed Ni (sites for carbon monoxide and hydrogen adsorption) , significantly improved CO methanation[76]. The supreme activity and stability of Ni/FSCe over Ni-Ce/KCC-1, Ni/KCC-1, FSCe and KCC, were from its suitable MSI between the Ni nanoparticles and the CeO_2 support, which helped to inhibit crystallite migration and provided protection against coking. The Ni/FSCe showed greatly enhanced catalytic capability with the CO conversion of 95.67% and the CH_4 yield of 91.20% at 400 °C.

4. Summary and perspectives

Overall, this feature article summarizes mesoporous oxide-supported metal nanoparticles/nanocluster and their interactions with CO and/or water in three different heterogeneous catalytic reactions: water-gas shift reaction, CO oxidation, and Fischer-Tropsch synthesis. It's been clear that the mesoporous oxide-supported metal catalysts with unique physicochemical properties, with tuned MSI during the reduction condition, have attracted many interests in a wide range of applications. Many *in situ* and *operando* spectroscopic characterization techniques such as DRIFTS, Raman spectroscopy, and X-ray spectroscopy (i.e., AP-XPS, XAS) have also been applied to characterize surfaces and adsorbed species and investigate MSI comprehensively. With the understanding of their interactions with water and CO, one could have insights into selecting appropriate mesoporous oxide-supported metal catalysts.

Potential future directions for studying or using the knowledge featured here on interactions of CO and/or H_2O with mesoporous oxide-supported metal catalysts include but not limited to the following:

(1) *Catalysts optimization*, to create more active sites on metal-support interfaces, by focusing on the support's selection and preparation methods to adjust metal loading and to control phase and facets of components in a catalyst. Table 1 shows that SBA -15 doped with two active metals is a better catalyst, with Ni/Zr-Ce on SBA-15 the best, than any other catalysts made of mesoporous support with monometallic clusters for WGS; 2.9 nm CeO_2-Pd NP on SBA-15, or high entropy alloy made of five kinds of metals show better CO oxidation activity; and 0.25% Sn doped on mesoporous Co_3O_4-Al_2O_3 demonstrated the highest CO conversion in F-T synthesis. All these suggest that mixed oxides, mixed doped metals and high-entropy materials[72] deserve to be further studied for optimizing catalysts tailoring to specific reactions.

(2) *In situ* and *operando characterization techniques* during catalytic reactions, such as the ones that involve CO and H_2O; and/or post-reaction analysis of the designed catalysts above, to obtain a more comprehensive picture of surface interaction with water and CO. Those advanced techniques include but are not limited to X-ray absorption near-edge structure (XANES) and extended X-ray absorption fine structure (EXAFS) for electronic structure of catalysts under *operando* conditions as they are closely related to the actual reaction condition. Probing molecules such as CO can be used to detect the changes of oxidation states and particle sizes of active metals on the catalysts *in situ*. When needed, one can apply high energy monochromatic light such as synchrotron as the radiation source, to reach higher resolution of spectra by reducing background noise under high pressure/*operando* conditions.

(3) *Machine-learning prediction* of interested reactions with CO/H_2O on, specifically, mesoporous oxide-supported metal catalysts, is lacking but will provide important guidance on their applications. In fact, machine-learning studies have been conducted on nano, but not mesoporous, materials[102] for reactions such as WGS[103], CO oxidation[104] and F-T reaction[105], to predict the new catalysts with better performance.

(4) *Tandem reactions*[106] by carefully designing selections of metal supported on OMMs due to the coexisting of CO, H_2, H_2O in syngas; and emerging reactions involve CO and H_2O on OMMS in energy storage such as fuel cell, battery etc.[11,21,107]

Short acronyms

AP-XPS: ambient-pressure X-ray photoelectron spectroscopy
DRIFTS: diffuse reflectance infrared Fourier transform spectroscopy
EMSI: electronic metal-support interaction
FDU: Fudan University
HEA: high entropy alloy
KIT: Korean Advanced Institute of Science and Technology
MA: mesoporous alumina
MCM: Mobil Composition of Matter
MMOs: mesoporous metal oxides
MSI: metal-support interaction
MSU: Michigan State University
NPs: nanoparticles
OMC: ordered mesoporous carbon
OMMs: ordered mesoporous materials
OMMOs: ordered mesoporous metal oxides
OMS: ordered mesoporous silica
PGM: platinum group metal
SBA: Santa Barbara
SDA: structure directing agent
TMO: transition metal oxides
TOF: turn-over frequency
XAFS: X-ray absorption fine structure
XANES: X-ray absorption near-edge structure

XAS: X-ray absorption spectroscopy

Author contributions

The manuscript was conceptualized by H.Y., written by L.L., discussed, and edited by L.L., L.F., R.A.H. and H.Y.

Conflicts of interest

There are no conflicts to declare.

Acknowledgements

H.Y. was supported by Louisiana Board of Regents under the contract number LEQSF (2023-24)-RD-D-06; L.F. was supported by NSF under the award number 2119688. R.A. H acknowledges the financial support of the U.S. – Israel Fossil Energy Center (FEC)- administered by the BIRD Foundation and funded by the Israeli Energy Ministry and the U.S. Department of Energy.

References

1 X. Li, Y. Huang and B. Liu, *Chem*, 2019, **5**, 2733–2735.

2 L. Luo, R. Hernandez, X. D. Zhou and H. Yan, *Appl. Catal. A Gen.*, 2021, **624**, 118330.

3 C. T. Kresge, M. E. Leonowicz, W. J. Roth, J. C. Vartuli and J. S. Beck, *Nature*, 1992, **359**, 710–712.

4 B. Szczęśniak, J. Choma and M. Jaroniec, *Chem. Commun.*, 2020, **56**, 7836–7848.

5 Y. Wei, W. Yang and Z. Yang, *Int. J. Hydrogen Energy*, 2022, **47**, 9537–9565.

6 Y. Cui, X. Lian, L. Xu, M. Chen, B. Yang, C.-E. Wu, W. Li, B. Huang and X. Hu, *Materials*, 2019, **12**, 276. DOI:10.3390/ma12020276.

7 B. K. Singh, S. Lee and K. Na, *Rare Met.*, 2020, **39**, 751–766.

8 M. Gao, L. Wang, Y. Yang, Y. Sun, X. Zhao and Y. Wan, *ACS Catal.*, 2023, **13**, 4060–4090.

9 Z. Fu, G. Zhang, Z. Tang and H. Zhang, *Catal. Surv. from Asia*, 2020, **24**, 38–58.

10 S. Fajal, S. Dutta and S. K. Ghosh, *Materials Horizons,* 2023, **10**, 4083-4138. DOI: 10.1039/d3mh00672g.

11 S. Li, H. Zhang, S. Li, J. Wang, Q. Wang and Z. Cheng, *Renew. Sustain. Energy Rev.*, 2024, **202**, 114641.

12 S. Singh, R. Kumar, H. D. Setiabudi, S. Nanda and D. V. N. Vo, *Appl. Catal. A Gen.*, 2018, **559**, 57–74.

13 H. J. Queisser, J. Michl, P. Jadhav, M. A. Baldo, T. H. Reilly, A. C. Kanarr, A. Mohanty, J. Sussman, J. Lee, M. A. Baldo, M. W. Wilson, A. Rao, R. H. Friend, N. C. Greenham, R. E. Merrifield, B. Domercq, B. Kippelen, S. Holdcroft, D. N. Congreve, N. J. Thompson, M. A. Baldo, S. Zhao, S. R. Scully, M. D. Mcgehee, P. Peumans, V. Andersson, F. Zhang, A. Yakimov, S. R. Forrest, V. Ern, J. L. Fave, C. Guthmann, M. Schott, Y. Saito, H. Shinohara, N. Koch, W. Gao, A. Wan, A. Kahn, Y. Hu, K. Tao, C. Wu, C. Zhou, H. Yin and S. Zhou, *Science*, 2013, **340**, 337–342.

14 X. Wu, J. Hu, J. Qi, Y. Hou and X. Wei, *Sep. Purif. Technol.*, 2020, **239**, 116511.

15 H. Frey, A. Beck, X. Huang, J. A. van Bokhoven and M. G. Willinger, *Science*, 2022, **376**, 4–8.

16 D. D. Suppiah, W. M. A. W. Daud and M. R. Johan, *Energy and Fuels*, 2021, **35**, 17261–17278.

17 F. Rezvani, D. Austin, D. Le, T. S. Rahman and S. L. Tait, *J. Catal.*, 2024, **438**, 115723.

18 S. Kristy, S. Svadlenak, A. S. Hoffman, S. R. Bare and K. A. Goulas, *Appl. Catal. B Environ.*, 2024, **342**, 123329.

19 T. M. Nyathi, M. I. Fadlalla and M. Claeys, *ChemCatChem*, 2024, **16**, 14. DOI:10.1002/cctc.202400285.

20 Y. Zou, X. Zhou, J. Ma, X. Yang and Y. Deng, *Chem. Soc. Rev.*, 2020, **49**, 1173–1208.

21 S. Thomas, A. Umar, R. T. Yunarti, R. Bakri, B. R. Putra, W. T. Wahyuni, A. Arifutzzaman, M. K. Aroua and M. Khalil, *Materials Today Communications*, 2024, **40**, 110152. DOI: 10.1016/j.mtcomm.2024.110152.

22 J. Tapia-Pérez, C. Ostos, C. Mendoza-Merlano, J. Arboleda-Echavarría and A. Echavarría-Isaza, *Environ. Technol. Innov.*, 2024, **35**, 103713.

23 M. Mosaad Awad, I. Hussain, O. Ahmed Taialla, S. A. Ganiyu and K. Alhooshani, *Energy Convers. Manag.*, 2024, **311**, 118508.

24 Q. Zhang, P. Yang, H. Zhang, J. Zhao, H. Shi, Y. Huang and H. Yang, *Appl. Catal. B Environ.*, 2022, **300**, 120729.

25 Y. Zhao, F. Dong, W. Han, H. Zhao and Z. Tang, *Microporous Mesoporous Mater.*, 2019, **273**, 1–9.

26 T. Gupta, Samriti, J. Cho and J. Prakash, *Mater. Today Chem.*, 2021, **20**, 100428.

27 R. Prins, *J. Catal.*, 2020, **392**, 336–346.

28 N. C. Horti, M. D. Kamatagi, S. K. Nataraj, M. N. Wari and S. R. Inamdar, *Nano Express*, 2020, **1**, 010022. DOI:10.1088/2632-959X/ab8684.

29 M. B. Leonard, T. Li and E. E. Rodriguez, *ACS Appl. Mater. Interfaces*, 2024, **16**, 38757–38767.

30 M. Dubey, S. Wadhwa, A. Mathur and R. Kumar, *Appl. Surf. Sci. Adv.*, 2022, **12**, 100340.

31 C. A. Chagas and M. Schmal, *Int. J. Hydrogen Energy*, 2022, **47**, 8858–8866.

32 I. Y. Kaplin, E. S. Lokteva, K. I. Maslakov, A. V. Tikhonov, A. N. Kharlanov, A. V. Fionov, A. O. Kamaev, O. Y. Isaikina, S. V. Maksimov and E. V. Golubina, *Appl. Surf. Sci.*, 2022, **594**, 153473.

33 S. J. Tauster, S. C. Fung and R. L. Garten, *J. Am. Chem. Soc.*, 1978, **100**, 170–175.

34 Y. Li, Y. Zhang, K. Qian and W. Huang, *ACS Catal.*, 2022, **12**, 1268–1287.

35 J. A. Farmer and C. T. Campbell, *Science*, 2010, **329**, 933–936.

36 A. M. Lacoste, I. S. Tiscornia, M. Bonne, L. Michelin, B. Lebeau and A. V. Boix, *Microporous Mesoporous Mater.*, 2021, **320**, 111094. DOI:10.1016/j.micromeso.2021.111094.

37 R. R. Poolakkandy and M. M. Menamparambath, *Nanoscale Adv.*, 2020, **2**, 5015–5045.

38 T. T. T. Ngo, E. Besson, E. Bloch, S. Bourrelly, R. Llewellyn, S. Gastaldi, P. L. Llewellyn, D. Gigmes and T. N. T. Phan, *Microporous Mesoporous Mater.*, 2021, **319**, 111036 DOI:10.1016/j.micromeso.2021.111036.

39 D. Zhao, J. Feng, Q. Huo, N. Melosh, G. H. Fredrickson, B. F. Chmelka and G. D. Stucky, *Science*, 1998, **279**, 548–552.

40 Y. Meng, D. Gu, F. Zhang, Y. Shi, H. Yang, Z. Li, C. Yu, B. Tu and D. Zhao, *Angew. Chemie - Int. Ed.*, 2005, **44**, 7053–7059.

41 S. A. Bagshaw, E. Prouzet and T. J. Pinnavaia, *Science*, 1995, **269**, 1242–1244.

42 C. Yu, Y. Yu and D. Zhao, *Chem. Commun.*, 2000, 575–576.

43 J. Jammaer, A. Aerts, J. D'Haen, J. W. Seo and J. A. Martens, *J. Mater. Chem.*, 2009, **19**, 8290–8293.

44 R. Ryoo, J. M. Kim, C. H. Ko and C. H. Shin, *J. Phys. Chem.*, 1996, **100**, 17718–17721.

45 Q. Li and Y. Zhou, *Molecules*, 2023, **28**, 2013.DOI: 10.3390/molecules28052013.

46 G. Collins, P. R. Kasturi, R. Karthik, J. J. Shim, R. Sukanya and C. B. Breslin, *Electrochim. Acta*, 2023, **439**, 141678.

47 M. R. Benzigar, S. N. Talapaneni, S. Joseph, K. Ramadass, G. Singh, J. Scaranto, U. Ravon, K. Al-Bahily and A. Vinu, *Chem. Soc. Rev.*, 2018, **47**, 2680–2721.

48 R. Ryoo, S. H. Joo and S. Jun, *J. Phys. Chem. B*, 1999, **103**, 7743–7746.

49 H. Li, W. Zhang, D. Liu and W. Li, *Emergent Mater.*, 2020, **3**, 315–329.

50 H. P. Lin, C. Y. Tang and C. Y. Lin, *J. Chinese Chem. Soc.*, 2002, **49**, 981–988.

51 A. Galarneau, M. Nader, F. Guenneau, F. Di Renzo and A. Gedeon, *J. Phys. Chem. C*, 2007, **111**, 8268–8277.

52 R. Ryoo and S. Jun, *J. Phys. Chem. B*, 1997, **101**, 317–320.

53 E. B. Celer, M. Kruk, Y. Zuzek and M. Jaroniec, *J. Mater. Chem.*, 2006, **16**, 2824–2833.

54 L. Luo, C. C. Oliver, I. M. Joseph, D. D. Gang, M. Chen, R. Hernandez and H. Yan, *Appl. Surf. Sci.*, 2022, **588**, 152866. DOI:10.1016/j.apsusc.2022.152866.

55 A. Pandey, P. Biswas, K. K. Pant and A. K. Dalai, *Ind. Eng. Chem. Res.*, 2024, **63**, 1000–1012.

56 S. Gupta and G. Deo, *Int. J. Hydrogen Energy*, 2023, **48**, 5478–5492.

57 H. Haji Andevary, A. Akbari, P. Safari, M. Omidkhah, A. Sharifi and M. Mirzaei, *Energy Fuels,* 2025, **39**, 1042–1051. DOI:10.1021/acs.energyfuels.4c04359.

58 F. Vaudry, S. Khodabandeh and M. E. Davis, *Chem. Mater.*, 1996, **8**, 1451–1464.

59 Y. Mo, C. Che, Z. Li, X. Zhao, K. Liu, B. Yang, X. Ren, L. A. Estudillo-Wong, J. Zang, J. Guan and Y. Feng, *Ind. Eng. Chem. Res.*, 2025, **64**, 3, 1567–1576. DOI:10.1021/acs.iecr.4c02529.

60 T. W. van Deelen, C. Hernández Mejía and K. P. de Jong, *Nat. Catal.*, 2019, **2**, 955–970.

61 P. Kraszkiewicz and W. Mista, *Catal. Commun.*, 2018, **110**, 14–17.

62 P. Kraszkiewicz, M. Małecka and W. Miśta, *Microporous Mesoporous Mater.*, 2022, **346**, 112338. DOI:10.1016/j.micromeso.2022.112338.

63 P. Hongmanorom, J. Ashok, S. Das, N. Dewangan, Z. Bian, G. Mitchell, S. Xi, A. Borgna and S. Kawi, *J. Catal.*, 2020, **387**, 47–61.

64 B. S. Yoon, K. J. Kim, E. H. Cho, H. R. Park, H. S. Roh and C. H. Ko, *Int. J. Hydrogen Energy*, 2023, **48**, 24894–24903.

65 N. S. Maboudi, F. Meshkani and M. Rezaei, *J. Energy Inst.*, 2021, **96**, 75–89.

66 Y. Xiao, C. Qu, X. Chen, W. Wang, X. Zheng and Q. Ye, *Chem. Eng. J.*, 2024, **488**, 151035.

67 D. Kim, D. Park, H. C. Song, B. Jeong, J. Lee, Y. Jung and J. Y. Park, *ACS Catal.*, 2023, **13**, 5326–5335.

68 P. R. Murthy, S. Munsif, J. C. Zhang and W. Z. Li, *Ind. Eng. Chem. Res.*, 2021, **60**, 14424–14433.

69 F. J. Méndez, M. G. Blanco, J. B. Rosas-Fernández and J. A. García-Macedo, *Microporous Mesoporous Mater.*, 2020, **305**, 110295. DOI:10.1016/j.micromeso.2020.110295.

70 Y. Li, J. Ying, T. He, G. Li, H. Zhang, S. Huang, T. Huang, W. Liu and H. Peng, *Ind. Eng. Chem. Res.*, 2023, **62**, 9159–9168.

71 H. Qin, Z. Yang, Q. Xia, PeifeiYao, C. Zheng, G. Lin, Z. Ye, S. Zhao and F. Yang, *Fuel*, 2023, **347**, 128290.

72 M. L. De Marco, W. Baaziz, S. Sharna, F. Devred, C. Poleunis, A. Chevillot-Biraud, S. Nowak, R. Haddad, M. Odziomek, C. Boissière, D. P. Debecker, O. Ersen, J. Peron and M. Faustini, *ACS Nano*, 2022, **16**, 15837–15849.

73 S. Badoga, G. Kamath and A. Dalai, *Appl. Catal. A Gen.*, 2020, **607**, 117861.

74 D. Shen, S. B. Han, X. Wang, M. Ali and J. W. Bae, *Catalysts*, 2022, **12**, 1447. DOI:10.3390/catal12111447.

75 N. Mohammad, R. Y. Abrokwah, R. G. Stevens-Boyd, S. Aravamudhan and D. Kuila, *Catal. Today*, 2020, **358**, 303–315.

76 A. H. Hatta, A. A. Jalil, M. Y. S. Hamid, N. S. Hassan, I. Hussain and N. W. C. Jusoh, *Fuel*, 2023, **333**, 126539.

77 S. Singh Negi, H. M. Kim, B. S. Cheon and D. W. Jeong, *Fuel*, 2024, **362**, 130908.

78 D. Jampaiah, D. Damma, P. Venkataswamy, A. Chalkidis, H. Arandiyan and B. M. Reddy, *Int. J. Hydrogen Energy*, 2023, **48**, 24860–24870.

79 X. P. Fu, C. P. Wu, W. W. Wang, Z. Jin, J. C. Liu, C. Ma and C. J. Jia, *Nat. Commun.*, 2023, **14**, 1–11.

80 F. Zaera, *Chem. Soc. Rev.*, 2014, **43**, 7624–7663.

81 L. Luo, J. D. LaCoste, N. G. Khamidullina, E. Fox, D. D. Gang, R. Hernandez and H. Yan, *Surf. Sci.*,

2020, **691**, 121486.

82 M. Sankar, Q. He, R. V. Engel, M. A. Sainna, A. J. Logsdail, A. Roldan, D. J. Willock, N. Agarwal, C. J. Kiely and G. J. Hutchings, *Chem. Rev.*, 2020, **120**, 3890–3938.

83 P. Yin, Y. Yang, H. Yan and M. Wei, 2023, DOI: 10.1002/chem.202203781.

84 D. Carta, T. Montini, M. F. Casula, M. Monai, S. Bullita, P. Fornasiero and A. Corrias, *J. Mater. Chem. A*, 2017, **5**, 20024–20034.

85 X. C. Sun, K. Yuan, W. De Hua, Z. R. Gao, Q. Zhang, C. Y. Yuan, H. C. Liu and Y. W. Zhang, *ACS Catal.*, 2022, **12**, 11942–11954.

86 M. Gao, Z. Yang, H. Zhang, J. Ma, Y. Zou, X. Cheng, L. Wu, D. Zhao and Y. Deng, *ACS Cent. Sci.*, 2022, **8**, 1633–1645.

87 S. Dey and G. C. Dhal, *Mater. Today Chem.*, 2020, **16**, 100228.

88 P. Chai, Z. Wu, L. Wu, H. Wang, C. Fu and W. Huang, *ACS Catal.*, 2022, **12**, 13292–13299.

89 G. Li, L. Li, Y. Yuan, J. Shi, Y. Yuan, Y. Li, W. Zhao and J. Shi, *Appl. Catal. B Environ.*, 2014, **158–159**, 341–347.

90 A. Holm, B. Davies, S. Boscolo Bibi, F. Moncada, J. Halldin-Stenlid, L. Paškevičius, V. Claman, A. Slabon, C. W. Tai, E. Campos dos-Santos and S. Koroidov, *ACS Catal.*, 2024, **14**, 3191–3197.

91 K. Liu, L. Liao and G. Liao, *Nanoscale*, 2024, **16**, 21783–21793.

92 X. Xu, S. K. Megarajan, Y. Zhang and H. Jiang, *Chem. Mater.*, 2020, **32**, 3–26.

93 C. Dong, X. Zong, W. Jiang, L. Niu, Z. Liu, D. Qu, X. Wang and Z. Sun, *Small Struct.*, 2021, **2**, 1–20.

94 J. Mosrati, A. M. Abdel-Mageed, T. H. Vuong, R. Grauke, S. Bartling, N. Rockstroh, H. Atia, U. Armbruster, S. Wohlrab, J. Rabeah and A. Brückner, *ACS Catal.*, 2021, **11**, 10933–10949.

95 M. V. Grabchenko, G. V. Mamontov, V. I. Zaikovskii, V. La Parola, L. F. Liotta and O. V. Vodyankina, *Appl. Catal. B Environ.*, 2020, **260**, 118148.

96 J. Liu, L. Wang, F. Okejiri, J. Luo, J. Zhao, P. Zhang, M. Liu, S. Yang, Z. Zhang, W. Song, W. Zhu, J. Liu, Z. Zhao, G. Feng, C. Xu and S. Dai, *ACS Catal.*, 2020, **10**, 8950–8959.

97 A. K. Dalai and B. H. Davis, *Appl. Catal. A Gen.*, 2008, **348**, 1–15.

98 J. Gahtori, G. Singh, C. L. Tucker, E. van Steen, A. V. Biradar and A. Bordoloi, *Fuel*, 2022, **310**, 122402.

99 F. Platero, S. Todorova, L. Aoudjera, L. Michelin, B. Lebeau, J. L. Blin, J. P. Holgado, A. Caballero and G. Colón, *ACS Appl. Energy Mater.*, 2023, **6**, 9475–9486.

100 N. Mohammad, S. Bepari, S. Aravamudhan and D. Kuila, *Catalysts*, 2019, **9**, 872 DOI:10.3390/catal9100872.

101 Z. Ren, Y. Cao, X. Yin, Y. Gan, R. Cai, Q. Wang, B. Feng, Y. Wu and X. Dai, *Fuel*, 2024, **363**, 130915.

102 J. Benavides-Hernández and F. Dumeignil, *American Chemical Society*, 2024, **14**, 11749-11779. DOI: 10.1021/acscatal.3c06293.

103 J. Chattoraj, B. Hamadicharef, Y. N. A. Syadzali, G. O. Limantara, Y. Zeng, C. K. Poh, L. Chen and T. L. Tan, *ACS Catal.*, 2023, **13**, 14334–14345.

104 M. S. Lifar, A. A. Tereshchenko, A. N. Bulgakov, S. A. Guda, A. A. Guda and A. V. Soldatov, *ACS Omega*, 2024, **9**, 27987–27997.

105 K. Motaev, M. Molokeev, B. Sultanov, V. Kharitontsev, A. Matigorov, M. Palianov, N. Azarapin and A. Elyshev, *Ind. Eng. Chem. Res.*, 2023, **62**, 20658–20666.

106 C. Wen, L. Lu, X. Zhang, K. Jin, L. Chen, Q. Zhang, L. Ma and C. Wang, *Fuel*, 2024, **357**, 129791.

107 L. Wang, B. Zhang, W. Zhou, Z. Zhao, X. Liu, R. Zhao, Z. Sun, H. Li, X. Wang, T. Zhang, H. Jin, W. Li, A. Elzatahry, Y. Hassan, H. J. Fan, D. Zhao and D. Chao, *J. Am. Chem. Soc.*, 2024, **146**, 6199–6208.

Data availability statements

No primary research results, software or code have been included, and no new data were generated or analyzed as part of this review.